

Excimer laser ablation of thin gold films on a quartz crystal microbalance at various argon background pressures

X. Zhang, S.S. Chu, J.R. Ho, C.P. Grigoropoulos

Department of Mechanical Engineering, University of California, MS 1740 Berkeley, CA 94720-1740, USA
(Email: cgrigoro@euler.berkeley.edu)

Received: 21 June 1996/Accepted: 9 December 1996

Abstract. Excimer laser ablation of gold films deposited on a quartz crystal microbalance is investigated. The ablation rate is directly obtained from the frequency shift of the microbalance. The measured single-shot ablation rate is found to be at least two orders of magnitude higher than the numerical predictions based on a surface vaporization model. Surface morphology studies indicate that hydrodynamic ablation plays a leading role in excimer laser ablation of thin gold films. In situ reflectivity and scattering measurements of the gold-film surface during the transient heating and melting upon excimer laser irradiation show that the melting duration is of microsecond order, which is much longer than the nanosecond melting duration in the case of a bulk target. This longer duration of melting may promote liquid motion, which leads to hydrodynamic ablation at a much higher rate compared with that of atomic vaporization from the surface. Experiments show that the ablation rate is also a strong function of the background gas pressure, which may be the result of the interactions between the gold vapor evaporated from the surface and the hydrodynamic motion in the molten gold.

PACS: 81.60; 85.40; 78.65; 44.10

Laser micromachining of thin-film materials has drawn great attention from many researchers in microelectronics and micromechanics for applications such as optical recording, circuit patterning, and mask generation [1–4]. The short pulse width and the strong intensity mean that the excimer laser can induce heating, melting, and vaporization of metals on a time scale of nanoseconds to microseconds. Localized ablation leads to precise micromachining of metallic thin films on dielectric substrates. Compared with visible and infrared pulsed lasers, an excimer laser offers unique advantages in micromachining of thin metallic films deposited on dielectric substrates. The coupling of excimer laser energy into the thin films can be greatly enhanced because the reflectivity of metallic thin films in the UV range is generally lower than in longer wavelength ranges. Recent progress in excimer laser manufacturing has provided higher beam output, larger

beam dimensions, and better homogeneity of the beam intensity distribution. These advances hold great promise even for broader applications in the fields of microelectronics and micromechanics.

In order to seek the optimal process conditions in excimer laser ablation of thin metallic films, better understanding of the physical process is needed for process design and control in an industrial environment. It has been shown that the surface topography growth is not significant during the first few pulses for the ablation of bulk metals because of the fast solidification of the molten layer due to the good heat transfer into the bulk solid [5, 6]. Compared with laser ablation of bulk materials, which for example is used in pulsed laser deposition of thin films, thin film ablation with an excimer laser is far more complicated. The distinct difference lies in the fact that due to the poor thermal conductivity of the underlying dielectric substrate, the laser energy is more confined within the metallic film, causing a substantially longer melting duration. The long period of the molten state in the thin film promotes both vaporization and hydrodynamic development.

Excimer laser ablation of metallic films with various laser wavelengths, fluences, and dielectric substrate combinations have been investigated, and several physical models have been proposed to explain the experimental observations [7–9]. The vaporization mechanism consists of atomic removal of particles from the surface at elevated temperatures during and after the excimer laser irradiation of thin metal films [10]. The explosion mechanism implies that instantaneous gasification occurs at the film–substrate interface, due to the high temperature reached across the film [11]. This model is essentially based on the mechanism of heterogeneous vapor nucleation at the interface. Thus the vapor explosion and the subsequent liquid expulsion contribute to ablation. The third model suggests that the ablation process is a combination of vaporization from the surface and hydrodynamic development of the molten surface during the prolonged melting [12, 13]. Recent high-speed photography in excimer laser irradiation and melting of copper thin films deposited on PMMA has indicated that the hydrodynamic motion, evolving over several microseconds, induces the removal of the thin film from the substrate [1]. On the other hand, the single-shot abla-

tion rate has been investigated at different laser fluences and wavelengths by Nd:YAG laser ablation of films deposited on the surface of a quartz crystal microbalance (QCM) [7]. The single-shot ablation rate has also been studied by measuring the ablated volume from excimer laser ablation by electron microscopy [5]. In contrast to other ablation rate measurement techniques, the measurement of mass loss from ablation of thin films deposited on a microbalance surface provides direct and precise detection of the total material removal, including vapor, liquid, and charged particles. It is noted that measurement of the total mass removal for a single-shot experiment is otherwise very difficult. However, previous work did not ensure laser beam homogeneity on the thin film and accurate determination of the laser ablation rate based on spatial acoustic response calibration. The details of single-shot laser ablation mechanisms remain unclear, and the possible connection between surface morphology growth and ablation rate has not been addressed yet.

In this work, excimer laser ablation of gold films deposited on a quartz crystal microbalance is studied at various background gas pressures with the intent to better understand the basic mechanisms involved in the ablation process. The influence of ablation spot geometry on single-shot ablation rate at various fluences is examined. The surface morphology on the ablated film is also examined by scanning electron microscopy. Computational modeling of surface temperatures, melting duration, and ablation-rate dependence on the irradiated laser fluence based on the surface vaporization mechanism is carried out for comparison. Additional reflectance and scattering diagnostics on the molten surface of the gold thin film at the melting threshold are applied to estimate the melt duration, which is an important factor in the hydrodynamic motion of the melt.

1 Experiment

The ablation rate experiment is carried out by focusing the excimer laser beam on thin gold films deposited on the surface of a quartz crystals microbalance (QCM). The microbalance is placed in a high vacuum chamber as shown in Fig. 1 with the pressures varying from 10^{-4} Pa to 5×10^4 Pa. The microbalance is capable of measuring thickness changes in the thin film deposited on or removed from the quartz crystal from a few angstroms to a few tens of microns depending on the material of the film. The principle of the microbalance operation is based on the fact that as an electric charge is applied, the natural frequency of a piezoelectric quartz crystal with a specific geometry will shift if the mass of the deposited thin film changes [14]. In most cases, the QCM is used for thickness measurement in thin-film deposition process monitoring. However, the etching mode in which the material removal is measured is not at all straightforward in the microbalance operation. The wafer geometry and the acoustic field distribution mean that mass removal at different locations on the quartz wafer causes a dramatically different frequency response. The nonlinear frequency response requires an additional calibration for the experiment.

The QCM system used in this experiment consists of three parts: the quartz crystal, an oscillator, and a monitor for measuring the change in the quartz crystal frequency as a result of deposition or etching (Fig. 1). The quartz crystals used are

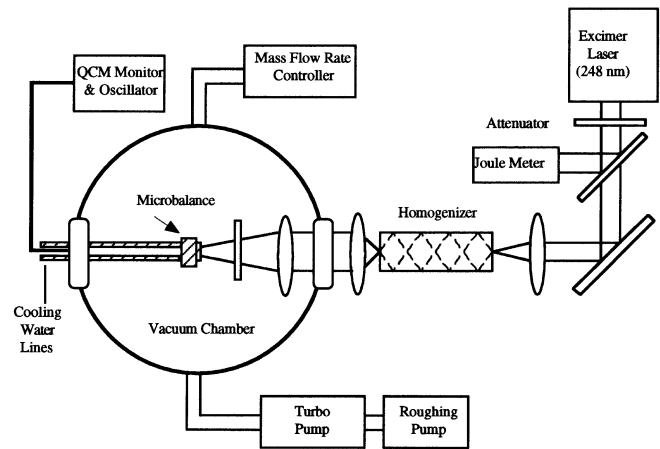


Fig. 1. Experimental setup for the measurement of the ablation rate in excimer laser ablation of thin film gold deposited on a quartz microbalance. System includes: a KrF excimer laser, UV optical delivery system, vacuum chamber with turbo and roughing pumps, and a quartz microbalance

6 MHz AT-cut wafers. A $0.54 \mu\text{m}$ thick gold film is deposited on the front surface of the crystal. Variations in the film thickness on the quartz crystals used in this experiment are limited to 4%. The experiments are performed in a vacuum chamber. Various background gas pressures are achieved by introducing argon gas (99.999%) through an automatic mass-flow controller. An industrial grade excimer laser (Lumonics Index 200) with pulse width of 26 ns (FWHM) is used in this work. The laser fluence is varied by adjusting the charging voltage in the laser and by a set of attenuators placed in the beam path. The optical delivery system is designed to form a uniform laser spot on the quartz crystal surface, which includes a $1 \text{ mm} \times 5 \text{ mm} \times 100 \text{ mm}$ tunnel-type homogenizer (90% uniformity), and 500 mm, 250 mm and 100 mm UV lenses. The irradiated spots are rectangles of about $0.4 \text{ mm} \times 2 \text{ mm}$ (aspect ratio 5 : 1) and $0.4 \text{ mm} \times 0.7 \text{ mm}$ (aspect ratio 1.75 : 1) in the center of the quartz crystal. Transmission through the entire beam delivery system is found to be about 45%. This optical design enables a maximum laser fluence of 12 J/cm^2 on the target surface. Before actual experiments can be performed, the spatial distribution of the frequency response of the quartz crystal is determined. The calibration was performed on the apparatus used in this experiment by ablating the gold film on the quartz crystal with a series of small spots as shown in Fig. 2a using the same fluence. Figure 2b shows the frequency change as a Gaussian function of distance from the center. The active area is essentially defined by an area within a 2 mm radius from the center. This Gaussian sensitivity distribution is in agreement with previously reported data obtained with the same technique [7] as well as by other methods [15, 16]. Once this distribution is established, the ratio of the frequency response of an ablated spot of any size and location to that of the entire aperture is determined by numerical integration. Therefore the mass removal at each laser pulse is accurately determined. The averaged ablation depth was used as the ablation rate by averaging the mass removal over the spot area.

The ablation rate experiment consisted of two parts. In the first part, each crystal was ablated at a specific laser fluence with a background Ar pressure of 10^{-4} Pa, 40 Pa, or 5×10^4 Pa. A fixed laser spot of $0.4 \text{ mm} \times 2 \text{ mm}$ on the gold

film was used. In the second part, each crystal was ablated with a smaller laser spot of $0.4 \text{ mm} \times 0.7 \text{ mm}$ at a background pressure of $5 \times 10^4 \text{ Pa}$. The smaller irradiated spot was achieved by masking the laser beam at the homogenizer exit. The geometry effects on ablation were studied by comparing the ablation-rate dependence on laser fluence for two different beam spot sizes. In this work, the single-shot ablation rate was obtained instead of using multiple pulses on the same spot in order to prevent possible influences due to surface morphologic changes after the first few pulses. A magnified photograph of each crystal was also analyzed to determine precisely the size and location of each spot in order to obtain an accurate sensitivity factor. Ablated surface morphologies of gold films were examined by SEM.

The melting duration was determined by measurement of both reflectance and scattering. These experiments were performed in air as shown in Fig. 3. A silicon diode sensor with nanosecond resolution was used to measure the reflected and scattered beam. An Ar^+ ion laser at 488 nm was used as the probe beam, and the intensities of the reflected and scattered light from the molten surface induced by the excimer laser irradiation of the gold film were monitored. The scattered light was measured similarly, except that a small solid angle confining the specular reflection was blocked. The remainder of the scattered beam was further focused on the silicon diode. The

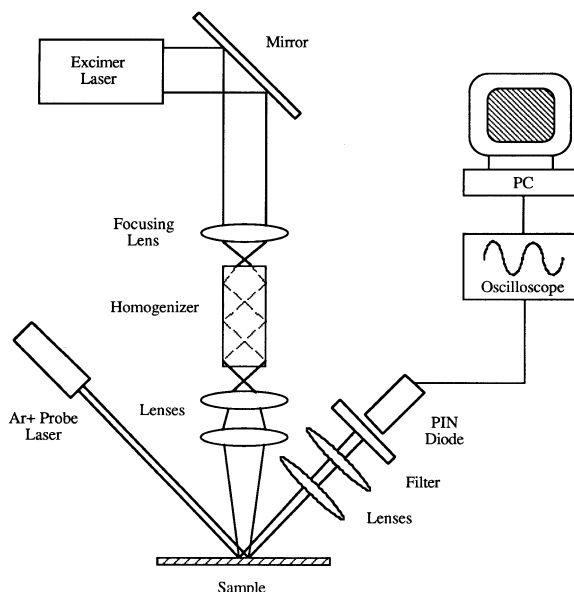


Fig. 3. Experimental setup for surface reflectivity and scattering measurement during the excimer laser heating and melting at melting threshold fluence. Setup includes: an excimer laser, UV beam delivery system, an Ar^+ laser as a probing beam, a PIN diode, an oscilloscope, and a PC for data acquisition

primary attention in this work, however, was on the laser fluence regime near the melting threshold, where molten surface morphology growth is not significant and ablation is minimal, in order to quantify the magnitude of the melting duration in the gold film.

2 Surface vaporization model

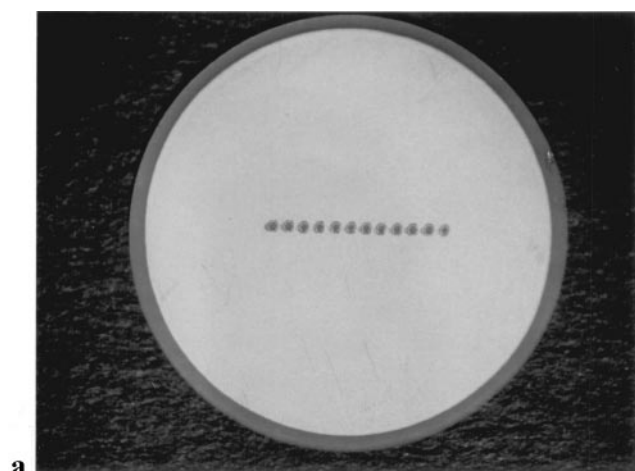
In order to gain a better understanding of the vaporization model as compared with the mechanism of hydrodynamical material removal near the threshold regime, a one-dimensional heat-conduction computation was employed to solve the phase transition and melting duration in the gold film deposited on a quartz substrate. The laser spot on the sample surface had a rectangular cross section of $0.4 \text{ mm} \times 2 \text{ mm}$, and the spatial distribution of the laser beam intensity was taken to be uniform. Since the laser spot was much larger than the gold film thickness, one-dimensional treatment in the computation was appropriate. The temporal distribution of the laser intensity, $I(t)$, was directly recorded from the KrF laser with a pulse duration of 42 ns and peak value at 18 ns . The fluence was adjusted between $0.6\text{--}0.9 \text{ J/cm}^2$ for comparison to the experimental values near the threshold.

The metal surface reflectivity at the wavelength of the excimer laser is given by the expression for normal light incidence:

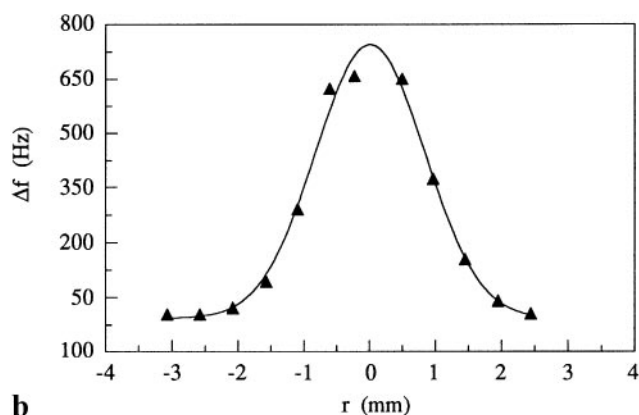
$$R = \frac{(n-1)^2 + k_{\text{ext}}^2}{(n+1)^2 + k_{\text{ext}}^2}, \quad (1)$$

where n and k_{ext} are the real and imaginary parts of the refractive index, and $n = 1.22$ and $k_{\text{ext}} = 1.49$ for Au. The absorption coefficient, α , is given by

$$\alpha = \frac{4\pi k_{\text{ext}}}{\lambda}. \quad (2)$$



a



b

Fig. 2a,b. Frequency sensitivity calibration of the quartz microbalance. **a** Images of 12 laser ablation spots were made along the diameter of the crystal, **b** corresponding frequency change on the quartz crystal for each spot as shown as dots and Gaussian fit as line

Here $\lambda (= 248 \text{ nm})$ is the wavelength of the KrF laser. The energy intensity absorbed by the Au thin-film target, Q_{ab} , which is treated as the source term in the energy equation, is given by

$$Q_{ab}(z,t) = (1-R)I(t)\alpha \exp(-\alpha z). \quad (3)$$

The laser absorption penetration depth is of the order of 10 nm, and the cross section of the laser beam is of the order of mm. Thus, the heat transfer in the target is reasonably approximated as a one-dimensional conduction problem described by

$$\rho(T)C_p \frac{\partial T}{\partial t} = \frac{\partial}{\partial z} \left(k(T) \frac{\partial T}{\partial z} \right) + Q_{ab}, \quad (4)$$

where k is the thermal conductivity (W/mK) of the film. The heat loss is primarily by thermal conduction through the film to the substrate. The heat loss from the Au surface to the ambient via thermal conduction, convection and radiation is negligible compared to the laser pulse duration. The boundary conditions (BC) can be set as $\partial T/\partial z|_{z=0} = 0$, and the temperature on the substrate bottom is the ambient temperature. The initial temperature of the target was set to be equal to the ambient temperature (initial condition (IC)).

The heat conduction equation, in the enthalpy formulation for the solution of phase change problems [17, 18], can be written as:

$$\frac{\partial h(T)}{\partial t} = \frac{\partial}{\partial z} \left(k(T) \frac{\partial T}{\partial z} \right) + Q_{ab}, \quad (5)$$

where h is the enthalpy and is a function of temperature, $h = h(T)$. The vaporization flux J_{ev} is described by

$$J_{ev} = n_0 \left(\frac{k_B T_s}{2\pi m_a} \right)^{1/2} \exp \left(-\frac{\varepsilon}{k_B T_s} \right), \quad (6)$$

where T_s is the surface temperature, m_a the weight of an atom, ε the latent heat of vaporization, k_B the Boltzmann constant, and n_0 the number density of the liquid gold at the liquid–vapor interface. The enthalpy equation and the associated BCs and IC are discretized by using a Crank–Nicolson formulation that incorporates temperature-dependent material properties. The transient surface temperature T_s is therefore obtained from the numerical calculation. The total ablation depth D due to surface vaporization can be obtained by integrating J_{ev} over time (ρ is the density of liquid gold):

$$D = \int_0^{\infty} J_{ev}(m_a/\rho) dt. \quad (7)$$

3 Results and Discussion

The dependence of the ablation depth on the excimer laser fluence at Ar background pressures of $5 \times 10^4 \text{ Pa}$, 40 Pa , and 10^{-4} Pa is shown in Fig. 4. The ablation depth increases monotonically from a few nanometers to 400 nanometers with laser fluence at all pressures. The experimental ablation thresholds range from 0.7 J/cm^2 to 0.9 J/cm^2 . However, according to the surface vaporization model, there is no definite ablation

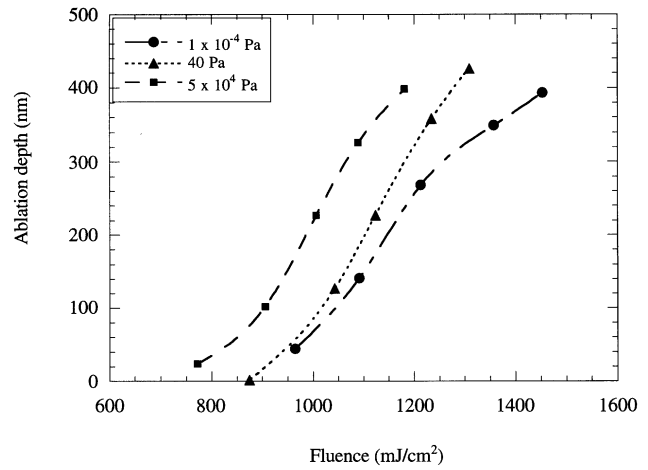


Fig. 4. Ablation rate dependence on laser fluence and argon gas background pressures for excimer laser ablation of thin film gold on a quartz microbalance

threshold during excimer laser heating, melting, and vaporization; the ablation is a continuous process at all temperatures that includes sublimation from the solid phase and vaporization from the liquid phase, although the ablation is predicted to increase dramatically with temperature. It is surprising to find that the ablation rate also strongly depends on the background pressure. It can be seen from Fig. 4 that at a fixed laser fluence, for example 1.1 J/cm^2 , the ablation rates are 150 nm/pulse , 200 nm/pulse , and 340 nm/pulse for background argon pressures of 10^{-4} Pa , 40 Pa , and $5 \times 10^4 \text{ Pa}$, respectively. With the increase in the background pressure, the ablation rate increases rapidly, whereas the ablation threshold decreases. The physical origin of this pressure dependence of the ablation rate is still not clear at this point.

It is impossible to predict this pressure dependence in the framework of purely surface vaporization [10]. In this model, the laser ablation of the thin film is described entirely as surface sublimation and vaporization during the transient heating of the thin film, which occur when the surface is subjected to intense excimer laser irradiation. The sublimation and vaporization rates of the surface material are primarily functions of the transient surface temperature and the melting duration, which are both determined by the excimer laser fluence and pulse shape, and by the optical and thermal properties of the thin films and substrates. However, the major contribution to the ablation rate arises from the molten surface as described by the term $\exp(-\varepsilon/k_B T_s)$. It is further assumed that the surface in the molten state remains as flat as the original film. The laser ablation rates predicted on the basis of this model at different laser fluences are less than one monolayer of gold per pulse, as shown in Fig. 5. Compared with the experimental values in Fig. 4, the computed ablation depth is at least two orders of magnitude smaller. This discrepancy clearly suggests that there must be other mechanisms incorporated in the laser thin-film ablation process.

The explosion mechanism describes the origin of the ablation process in terms of vaporization at the film–substrate interface. This model is more likely to be relevant for the case where the substrate has a lower melting or decomposition point than that of the thin-film material, so that the vaporization and subsequent explosions at the interface can become much more pronounced. However, the explosion mechanism

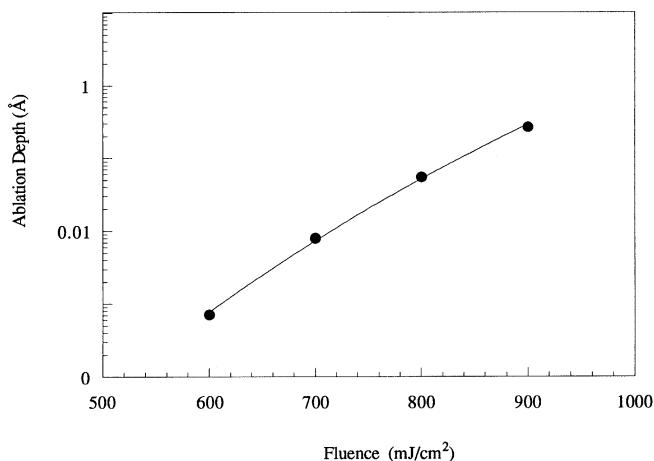


Fig. 5. Computed ablation rate dependence on laser fluence based on the surface thermal vaporisation model for excimer laser ablation of thin film gold on a quartz wafer

is not a likely source for ablation in this experiment since the substrate quartz crystal has a much higher melting point (1996 K) than the gold film (1338 K).

The hydrodynamic mechanism accounts for laser ablation of thin films by the hydrodynamic development of the molten film induced by the laser irradiation. Laser ablation via this mechanism can be divided into two parts. First, the vaporization dominated ablation starts at the early stage of laser heating and melting of the gold film, though the rate is very low at this stage. Second, these vaporized atomic particles interact with the ambient gas immediately so that a gold vapor cloud is confined close to the surface, resulting in a local pressure region near the film surface. For the larger background Ar pressures, the local pressure exerted on the liquid film is higher than that in the case of the lower background pressure. This local pressure enhances the formation of surface hydrodynamic instabilities and results in the ablation of liquid in the form of droplets. It is therefore expected that the hydrodynamic ablation of the thin film is dependent on the background gas pressure.

To seek further explanations for the apparent inconsistency in ablation depth between Figs. 4 and 5, surface morphologies were studied by SEM. Figure 6a shows a surface of the thin gold film subjected to a laser fluence of 0.9 J/cm^2 at a pressure of 40 Pa. The ablation rate measured by the microbalance at this fluence is very small as shown in Fig. 4. This is also confirmed by the morphology of the surface shown in Fig. 6a. The surface is frozen from the molten phase, exhibiting waves with wavelengths on the order of microns. However, as the laser fluence is increased, the gold films undergo dramatic changes, and the surface morphology becomes quite different as shown in Fig. 6b. The edge definition of the spot is still sharp in Fig. 6b, which demonstrates good optical alignment in the system and uniform intensity across the laser beam. However, droplets of gold are observed on the irradiated spot as if they are left behind by a splash. This indicates that the surface ablation is most likely to be the result of the hydrodynamic motion of liquid gold during and after the laser pulse, instead of simple surface sublimation and vaporization. A transition region is observed at the edges of the irradiated spot on the gold film. Although the center of the spot is highly ablated, less gold is removed close to the edges. The surface morphologies range

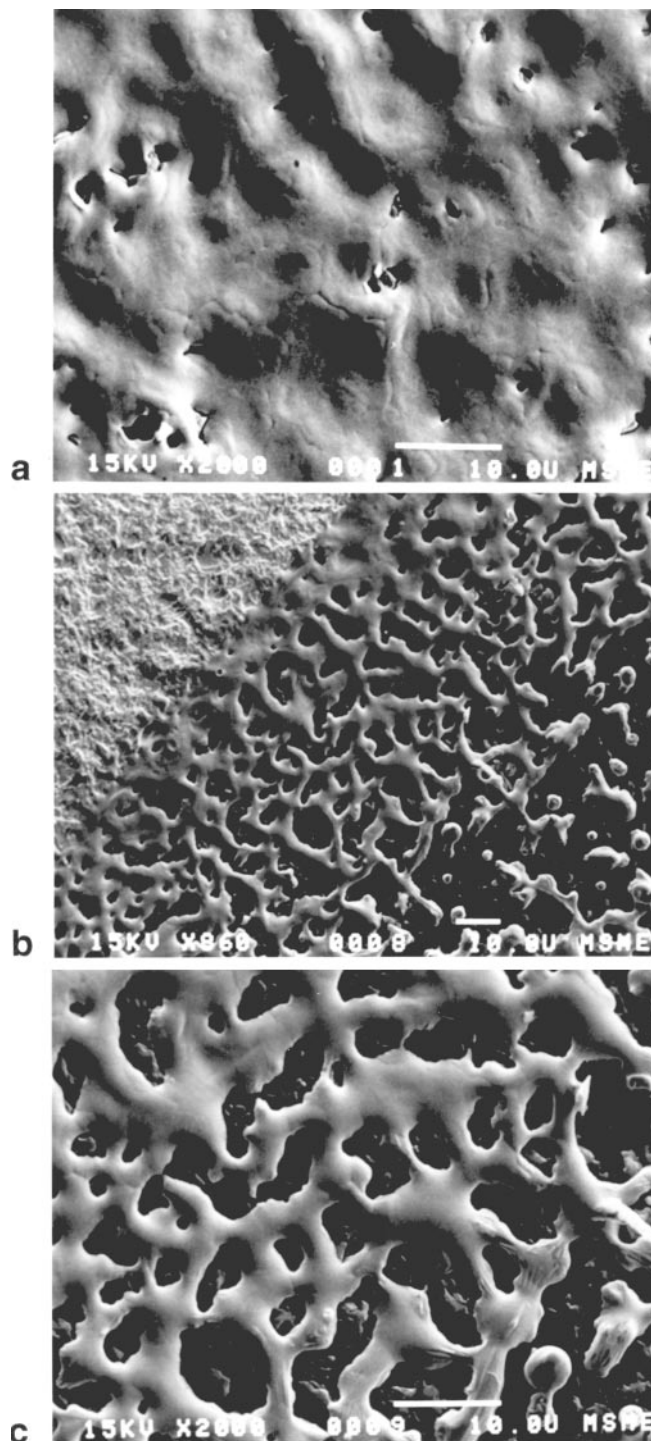


Fig. 6a-c. Surface morphology of the laser irradiated thin film gold on a quartz substrate. **a** A molten surface without substantial ablation at 0.9 J/cm^2 and 40 Pa; **b** an ablated surface at 1.1 J/cm^2 and 40 Pa; **c** an ablated surface at 0.9 J/cm^2 and $5 \times 10^4 \text{ Pa}$

from mostly flat resolidification near the edges, to network-like separations in a transition region, and to micron-sized droplets in the center part of the laser spot. This observation also supports the hydrodynamic mechanism during the ablation of the thin film effected by a single pulse, which is proposed based on observations at near-threshold laser sputtering of bulk gold, after a few thousand pulses [19]. The temperature is lower for the material close to the edges than

for the center part of the irradiated spot because of the lateral heat diffusion through the unirradiated solid gold film. Thus the surface tension of the melt near the edges is larger than in the center part, suppressing the pronounced hydrodynamic motion of the melt. Laser-ablated surface morphologies under the same laser fluence of 0.9 J/cm^2 , but different background pressures, were also examined as shown in Figs. 6a,c. It is clearly seen that, at higher background pressures ($5 \times 10^4 \text{ Pa}$), the gold films were substantially ablated. The surface morphology indicates that hydrodynamic ablation occurred. This observation is also consistent with the dependence of the ablation rate on the background pressure measured by the QCM, shown in Fig. 4.

Compared with excimer laser ablation of bulk gold, the hydrodynamic effect is very strong in thin films. In the bulk case, surface morphology does not grow until after many pulses. Surface growth is a cumulative process, because the melting duration induced by the excimer laser is quite short (of the order of 100 ns). In the laser ablation of thin films, however, the melting duration can last much longer than in the bulk, because the heat generated by the laser irradiation cannot dissipate quickly through the quartz substrate, which has a much lower thermal diffusivity than gold. One-dimensional computation results on the transient surface temperature of a gold film subjected to different laser fluences is shown in Fig. 7. It can be seen that the surface melting commences during the laser pulse (of 26 ns) and that the melt duration can last for a few microseconds. Cooling of the surface to ambient temperature after solidification, however, requires more than ten microseconds. Even though this model does not include any hydrodynamic effects on the heat transfer and phase change processes, it does give a general picture of the onset and duration of gold-film melting. The time scale of the hydrodynamic motion of the molten gold is obviously limited to the melt duration. The prolonged melt duration of the gold film provides more time for hydrodynamic development, consequently further supporting for the possibility of hydrodynamically induced ablation. Hydrodynamic ablation implies that material is removed in the form of clusters, droplets, or other macroscopic formations. Therefore, the hydrodynamic ablation rate can be much higher than the surface vaporization

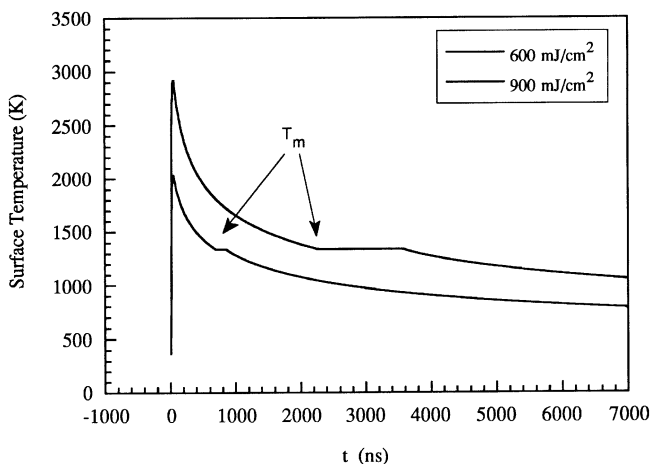


Fig. 7. Transient surface temperature of the gold film on quartz wafer during and after excimer laser irradiation at two laser fluences: 600 mJ/cm^2 and 900 mJ/cm^2 , computed based on the surface thermal vaporisation model

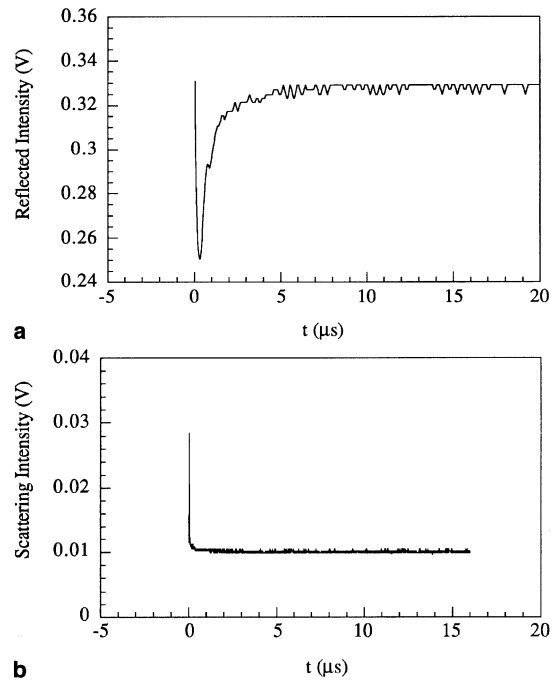


Fig. 8. **a** Reflectivity and **b** scattering from the surface of thin film gold probed by an Ar^+ beam during excimer laser irradiation of thin film gold on quartz wafer at laser fluence 0.61 J/cm^2

rate, as shown by the comparison of the experimental values in Fig. 4 and the computational results in Fig. 5.

Experimental investigations into the surface reflectivity of the gold films at $\lambda = 488 \text{ nm}$ (excimer laser irradiation) were carried out near the surface melting threshold (610 mJ/cm^2). Generally, surface reflectivity is a function of the optical properties of the materials, which may also be temperature dependent. Earlier studies on the optical properties suggest that the metal surface reflectivity generally does not change much before melting. However, measurements of dielectric constants and electrical conductivities in both solid gold and liquid gold predict a drop in reflectivity of over 25–30% at $\lambda = 488 \text{ nm}$ from 573 K to the melting point at 1390 K [20]. This provides a reasonable basis for developing a qualitative determination of the melt duration in this experiment. It is shown in Fig. 8a that surface reflectivity measured at a laser fluence of 610 mJ/cm^2 drops and recovers within a few microseconds, thus suggesting that the melting duration is also of the order of a few microseconds. An exact determination of the melting duration by probing the reflectivity requires detailed knowledge of the dependence of the optical properties (at $\lambda = 488 \text{ nm}$) on temperature in both the solid and the liquid phases. The change in the reflectivity observed is about 26%. It is important to make sure that the reflectivity drop is not due to the surface deformation in either the solid or the liquid states. The reflected signal from the surface due to surface scattering was therefore examined under the same conditions as in the reflectivity measurement. The scattering signal is found to be very small compared to the directly reflected signal over the melting duration suggested by the reflectivity experiment and the numerical results, as shown in Fig. 8b. This indicates that the surface remains relatively flat during heating and melting at a fluence just above the melting threshold. Therefore, it is likely that the 26% reflectivity drop observed originates from the change in optical properties

during melting. The reflectance and scattering measurements at the melting threshold reveal that the melting duration resulting from excimer laser irradiation of gold films is of the order of a few microseconds, which is also predicted by the purely thermal model. It is noted here that this consistency in the melting duration near the melting threshold indicates only that the purely thermal model provides a reasonable description of the surface phase condition in this regime. However, the prediction of the melting duration alone does not imply that the purely thermal model is a dominant mechanism in the laser ablation of the thin films, which develops later on and at higher fluences. This finding, namely a microsecond melting duration in the interaction of the excimer laser with gold films, is important because the long melting duration provides an opportunity for hydrodynamic development in the melt, which eventually leads to hydrodynamic ablation.

The influence of the laser-spot geometry on the ablation rate was investigated. The ablation characteristics are quite different for the two geometries studied, as shown in Fig. 9. For the $0.4 \text{ mm} \times 2 \text{ mm}$ geometry (5 : 1 aspect ratio), the ablation threshold is about $0.6\text{--}0.7 \text{ J/cm}^2$, with the ablation rate increasing quickly as the laser fluence goes up. However, for the $0.4 \text{ mm} \times 0.7 \text{ mm}$ geometry (1.75 : 1 aspect ratio), the ablation threshold is at 1.2 J/cm^2 ; the entire ablation curve is delayed by $\Delta\Phi = 0.4\text{--}0.5 \text{ J/cm}^2$ compared with the 5 : 1 ratio geometry. The ablation rate was accurately determined by integrating the frequency response of the spot at any size and location according to the Gaussian sensitivity distribution shown in Fig. 2b. The possible influence from the laser beam homogeneity (90%) was also examined and ruled out for the large shifts in the ablation threshold observed in Fig. 9. This phenomenon may be related to the nature of the hydrodynamic mechanism, where two-dimensional fluid motion is greatly affected by the boundaries. It is observed that the liquid gold tends to form spherical beads on the quartz substrate as shown in Fig. 6b, which is driven by the tendency to minimize the surface energy of the molten system. For the larger ratio of 5 : 1, the molten rectangular film geometry is far from the equilibrium shape, which is circular in the 2D case. The tendency to reach the circular shape is therefore much larger for the 5 : 1 ratio configuration than for the 1.75 : 1 geometry, which is closer to being circular. This tendency can drive

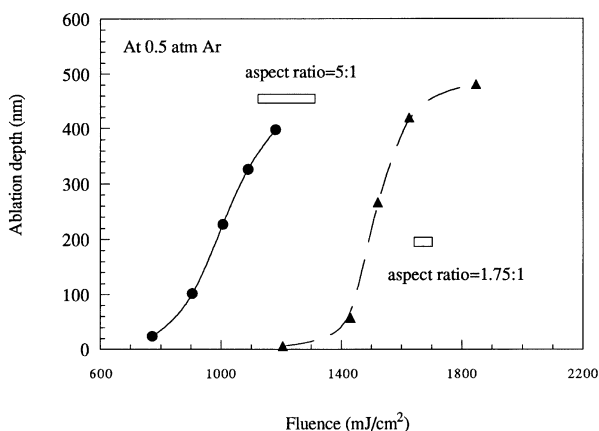


Fig. 9. Influence of the ablation spot geometry on ablation rate dependence over the laser fluence range $0.6\text{--}2.0 \text{ J/cm}^2$ at 0.5 atm argon background pressure; two spot geometries with aspect ratios of 5 : 1 and 1.75 : 1, respectively

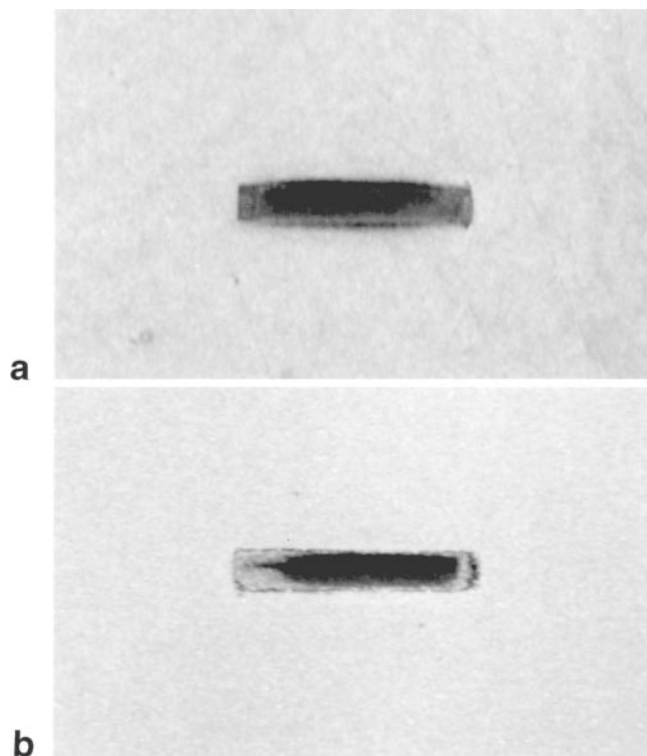


Fig. 10a,b. Ablated surface morphology: **a** formation of brown edges around the spot by laser ablation at 0.5 atm argon background gases; **b** no formation of brown edges around the spot by laser ablation at 40 Pa argon background gases

the longer side of the 5 : 1 spot to contract to the center. The ensuing acceleration of the liquid motion from the long side may cause collisions between the fluid lumps, thus leading to substantial material ablation. In contrast, for the 1.75 : 1 ratio geometry, the tendency to retreat to the circular shape is smaller. The slower acceleration of the fluid is correspondingly less significant in causing ablation.

For ablation of gold films in a $5 \times 10^4 \text{ Pa}$ Ar background, the edges around the ablation spot appear to be brown, as shown in Fig. 10a, when examined under an optical microscope. The brown edges do not appear in ablation at the lower background pressures of 40 Pa and 10^{-4} Pa as shown in Fig. 10b. This phenomenon suggests that there could be plasma ignition at the higher background pressure. It is possible that during the initial stage, gold-vapor molecules released from the surface with large kinetic energy collide with the surrounding Ar atoms, thus producing a layer of hot Ar atoms at temperatures at which thermal plasma ignition is possible. Though the interactions between the Ar plasma, the Au vapor, and the molten Au surface are very complicated, it is expected that the hydrodynamic ablation of the thin molten gold can be affected by the presence of such a plasma. In ablation at lower background pressures, the Au vapor is not confined in a thin layer as is the case for ablation at higher background pressures. Furthermore, the collisions between the Au and Ar atoms are reduced because of the diluted Au vapor and the lower Ar density, at lower background pressures. Therefore, plasma formation is more difficult at lower Ar background pressures. In future work, it will be interesting to study in detail the possibility of Ar plasma formation in the laser ablation of thin films at different background pressures.

4 Conclusion

Excimer laser ablation of gold films deposited on quartz crystals at different Ar background pressures has been studied. Calibration of the microbalance was carried out across the quartz crystal surface. A Gaussian sensitivity distribution was found, which was approximately 2 mm in width. The ablation rate was obtained by measuring the natural vibration frequency of the quartz crystal in the microbalance. It was found that the ablation rate depends strongly on the background pressure and the laser fluence. A one-dimensional numerical model was developed based on a simple surface vaporization mechanism and was used to predict the surface temperature and melting duration. The measured single-shot ablation depth was found to at least two orders of magnitude larger than predictions from the surface vaporization model. This finding demonstrates that the ablation of the film was not due to surface vaporization alone. Surface morphology observed by SEM indicated the existence of melting and hydrodynamic motion in the thin molten gold film. An Ar⁺ laser probe beam was used to measure the surface reflectivity and scattering just above the melting threshold fluence. It was found that the melting duration is of microsecond order, manifested by a reflectivity drop of 26% during melting, which is close to the theoretical prediction from the measured dielectric constant and electric conductivity. The small scattering signal suggests that the measured reflectivity drop was due to the phase change in the thin film, rather than due to the scattering loss caused by surface deformation. The measured melt duration of microsecond order is consistent with the computed value based on transient heating and melting upon laser irradiation. This prolonged melt duration is expected to promote hydrodynamic development of thin molten gold and lead to a much higher ablation rate as observed. The hydrodynamic mechanism is therefore proposed for the ablation of gold films in order to explain the single-shot ablation rate observations. The existence of a longer melt duration in gold films due to the poor thermal conductivity of the quartz substrate supports this proposition. Hydrodynamic development induced by instabilities during the long melt duration leads to substantial ablation in macroscopic form, such as droplets instead of atomic vaporization from the surface. The experiments showed that the ablation rate was also a strong function of the background gas pressure, which may be the result of interactions between the Au vapor from the surface and the hydrodynamic motion in the molten Au. The influence of the ablated spot geometry on the ablation rate of the Au film was also studied. A larger aspect ratio (5 : 1) tended to be easier to ablate compared with a smaller aspect ratio (1.75 : 1). A possible explanation is made based on the tendency of the molten film to minimize its surface energy by evolving to a circular two-dimensional shape. Brown edges around the spot are found only for the laser ablation of thin gold films at 5×10^4 Pa background Ar pressure,

and not at 40 Pa and 10^{-4} Pa. Possible Ar plasma ignition at higher background pressure is suspected to be responsible for this phenomenon.

Acknowledgements. Support to this work by the National Science Foundation under Grant No. CTS-9402911 is gratefully acknowledged.

References

1. H. Hayashi, I. Miyamoto: *Process of thin Cu film by KrF excimer laser*, Rev. of Laser Eng. **23**(12), 1081-1089 (1995)
2. Z. Toth, B. Hopp, Z. Kantor, F. Ignacz: *Dynamics of excimer laser ablation of thin tungsten films monitored by ultrafast photography*, Appl. Phys. A **60**(5), 431-436 (1995)
3. J. Solis, K.A. Rubin, C. Ortiz: *Structure and optical transformations by laser irradiation of InSb-based thin films*, J. Mater. Res. **5**(1), 190-210 (1990)
4. V.P. Veiko, I.M. Karpman, M.N. Libenson, E.B. Yakovlev: *Optimal regime for forming topological patterns when processing films with laser radiation*, Sov. J. Quant. Elec. **12**(11), 1408-1411 (1982)
5. R. Kelly, J.J. Cuomo, P.A. Leary, J.E. Rothenberg, B.E. Braren, C.F. Aliotta: *Laser sputtering—Part I. On the existence of rapid laser sputtering at 193 nm*, Nucl. Instrum. Methods B **9**, 329-340 (1985)
6. T.D. Bennett, C.P. Grigoropoulos, D.J. Krajnovich: *Near-threshold laser sputtering of gold*, J. Appl. Phys. **77**(2), 849-864 (1995)
7. J. Perez, B.R. Weiner: *The laser ablation of gold films at the electrode surface of a quartz crystal microbalance*, Appl. Surf. Sci. **62**, 281-285 (1992)
8. J.E. Andrew, P.E. Dyer, R.D. Greenough, P.H. Key: *Metal film removal and patterning using a XeCl laser*, Appl. Phys. Lett. **43**(11), 1076-1078 (1983)
9. V.P. Veiko, A.I. Kaidanov, M.N. Libenson, B.M. Yurkevich: *Destruction of absorbent films under the action of laser irradiation*, Elektronnaya Obrabotka Materialov **6**, 23-26 (1983)
10. U.C. Paek, A. Kestenbaum: *Thermal analysis of thin-film micromachining with lasers*, J. Appl. Phys. **44**(5), 2260-2268 (1973)
11. V.J. Zaleckas, J.C. Koo: *Thin film machining by laser-induced explosion*, Appl. Phys. Lett. **31**(9), 615-617 (1977)
12. V.P. Veiko, S.M. Metev, A.I. Kaidanov, M.N. Libenson, E.B. Yakovlev: *Two-phase mechanism of laser induced removal of thin absorbing films: I. Theory*, J. Phys. D. **13**, 1565-1570 (1980)
13. V.P. Veiko, S.M. Metev, K.V. Stamenov, H.A. Kalev, B.M. Jurkevitch, I.M. Karpman: *Two-phase mechanism of laser induced removal of thin absorbing films: II. Experiment*, J. Phys. D. **13**, 1571-1575 (1980)
14. G.Z. Sauerbrey: *Verwendung von Schwingquarzen zur Wägung dünner Schichten und zur Mikrowägung*, Z. Phys. **155**, 206-222 (1959)
15. P.J. Cumpson, M.P. Seah: *The quartz crystal microbalance; radial/polar dependence of mass sensitivity both on and off the electrodes*, Meas. Sci. Technol. **1**, 544-555 (1990)
16. M.D. Ward, E.J. Delawski: *Radial mass sensitivity of the quartz crystal microbalance in liquid media*, Anal. Chem. **63**, 886-890 (1991)
17. D.R. Atthey: *A finite difference scheme for melting problems*, J. Inst. Math. Applics. **13**, 353-366 (1975)
18. N. Shamsundar, E.M. Sparrow: *Analysis of Multidimensional Conduction Phase Change via the Enthalpy Model*, J. Heat Transfer, **97**, 333-340 (1975)
19. R. Kelly, J.E. Rothenberg: *Laser sputtering—Part II. The mechanism of the sputtering of metals low energy densities*, Nucl. Inst. Methods B **7/8**, 755-763 (1985)
20. J.C. Miller: *Optical properties of liquid metals at high temperatures*, Phil. Mag. **20**, 1115-1132 (1969)